Journal of Power Sources 196 (2011) 6651–6656

Contents lists available at ScienceDirect

Journal of Power Sources

journal homepage: www.elsevier.com/locate/jpowsour

Crystal and electronic structure change determined by various method for delithiation process of $Li_x(Ni,Mn)O_2$-based cathode material

Oki Sekizawa, Takuya Hasegawa, Naoto Kitamura, Yasushi Idemoto*

Department of Pure and Applied Chemistry, Faculty of Science & Technology, Tokyo University of Science, 2641 Yamazaki, Noda-shi, Chiba 278-8510, Japan

ARTICLE INFO

Article history:
Received 25 August 2010
Received in revised form
23 December 2010
Accepted 7 January 2011
Available online 19 January 2011

Keywords:
Li-ion battery
Crystal structure
Electronic structure
Chemical delithiation

ABSTRACT

We investigated effects of delithiation on crystal, electronic structure, thermodynamic stability and physical property of $Li_xNi_{0.5}Mn_{0.5}O_2$ by using a chemical delithiation treatment with ammonium peroxodisulfate, and compared the results with those of electrochemical delithiation. X-ray diffraction and thermodynamic data indicated that there was no phase transition in the samples after the chemical delithiation treatment within the lithium range of $0.50 \leq x \leq 1.00$. From the ICP measurements and potentiometric titration, it was found that the chemical treatment successfully remove Li from the structure without any elution of Ni and Mn, but it accompanied O_2 removal at an initial process of the delithiation, i.e. $0.80 \leq x \leq 1.00$. Crystal and electronic structure analyses also suggested such a O_2 removal at the lithium content range in the chemical delithiation method, although the estimated structure changes below $x = 0.80$ showed similar tendencies to those by the electrochemical delithiation.

1. Introduction

Secondary batteries are applied for many electronic devices widely like a cellular phone and the car battery. Especially, various researches are performed as for the Li ion battery, because of high energetic density, good cycle performance and light weight. As the cathode materials layered rock-salt structure $LiCoO_2$ [1], spinel structure $LiMn_2O_4$ [2], and olivine structure $LiFePO_4$ [3] has been put to practical use [4].

Co-free layered rock-salt structure $LiNi_{0.5}Mn_{0.5}O_2$ [5,6] is studied as the one of the alternative materials of these cathodes from the point of view of higher theoretical discharge capacity and higher thermostability [5–22]. Generally, the material including Ni^{2+} has cation mixing to some extent because Ni^{2+} and Li^+ ionic radii are very close. $LiNi_{0.5}Mn_{0.5}O_2$ in which Ni^{2+} and Mn^{4+} occupies 3b site one half each which composes transition metal layer is reported to have ca. 10% cation mixing [7–11,20–21]. Moreover, because there are some types of local structure caused by Ni/Mn order, many studies on them are performed by pair distribution function (PDF) which uses neutron total scattering, simulation by reverse Monte Carlo (RMC) method and ab initio calculation [7,8,12,20,22].

In this $LiNi_{0.5}Mn_{0.5}O_2$, Li intercalates and deintercalates along with charge–discharge cycle and it is well known that crystal structure changes complicatedly by Li migration. As a study of charge–discharge process, X-ray diffraction [13–15] and X-ray absorption [16–18] using synchrotron X-ray, X-ray photoelectron spectroscopy [19] (in situ measurements), and neutron diffraction [20] (ex situ measurement) were reported in terms of $LiNi_{0.5}Mn_{0.5}O_2$.

Previously, we reported the crystal structure and the thermodynamic stability of $Li(Ni_{1/3}Co_{1/3}Mn_{1/3})O_2$ after chemical delithiation treatment by using Rietveld refinement and calorimetry [23]. Chemical delithiation process by ammonium peroxodisulfate can make electrochemical delithiate state (charge state) by removal of Li from composition [24]. This process makes it easier to conduct neutron measurement of charged cathode materials compared with an electrochemical delithiation process, because of negligible effect of additional substances (e.g. AB and PVdF) and facile preparation of large sample quantities in the case of the chemical delithiation, and thus we can investigate detail of structure changes at delithiated state. Neutron shows not only clear scattering from light elements like Li and O, but also can distinguish elements with close atomic number like Ni and Mn. Considering this, it can be said that the structure analysis using neutron diffractions is one of the most suitable techniques to investigate the structural change in the charge–discharge.

There are some reports of chemical delithiation treatment using various oxidizing agent; for example, NO_2PF_6 and NO_2BF_4 used for $LiCoO_2$ [25], $Li(Ni,Co)O_2$ [25,26], $LiMn_2O_4$ [25] and $Li(Ni,Mn)O_2$ [27], $Na_2S_2O_8$ used for $LiCoO_2$ [28], $(NH_4)_2S_2O_8$ used for $LiMnO_2$ [24] and $Li(Mn_{1/3}Co_{1/3}Ni_{1/3})O_2$ [23], H_2SO_4 used for $LiMn_2O_4$ [29] etc. For $LiNi_{0.5}Mn_{0.5}O_2$, Venkatraman et al. used NO_2BF_6 and reported the results of composition and valence analysis, FTIR and Rietveld analysis [27]. Furthermore, it was also reported by

* Corresponding author. Tel.: +81 4 7122 9493; fax: +81 4 7123 9890.
E-mail address: idemoto@rs.noda.tus.ac.jp (Y. Idemoto).

0378-7753/$ – see front matter © 2011 Elsevier B.V. All rights reserved.
doi:10.1016/j.jpowsour.2011.01.018

Chebiam et al. that oxygen content showed different behavior in different material even by using same oxidizing agent [25]; that is, oxygen was removed at $0 \le x \le 0.8$ in Li_xCoO_2, $0 \le x \le 0.4$ in $Li_xNi_{0.85}Co_{0.15}O_2$ and oxygen was not removed in $Li_xMn_2O_4$. From these results, it seems that the oxygen shows different behavior by a combination of a sample and an oxidizing agent.

From such background, in this study, we prepared the $Li_xNi_{0.5}Mn_{0.5}O_2$ samples after chemical delithiate treatment and investigate average and local crystal structures, thermodynamic stability and electronic structure of the samples by structure analyses with neutron and synchrotron X-ray sources.

2. Experimental

2.1. Samples preparation

$LiNi_{0.5}Mn_{0.5}O_2$ were prepared by solid-state method. $LiOH{\cdot}H_2O$ (99.9%, Wako Pure Chemical Industries, Ltd.), MnO_2 (99.5%, Wako Pure Chemical Industries, Ltd.), and $Ni(OH)_2$ (99.9% Wako Pure Chemical Industries, Ltd.) were used as starting materials. These materials were mixed for 24 h, and then the precursor was obtained. Then this precursor was calcined at 650 °C for 24 h in air. After that, the powder was pressed into pellet at 40 MPa and sintered 950 °C for 15 h in air.

We removed Li from samples by chemical process with ammonium peroxodisulfate [24]. 1.0 g of $LiNi_{0.5}Mn_{0.5}O_2$ was immersed into 0.5 mol dm^{-3} of $(NH_4)_2S_2O_8$ (98.0%, Wako Pure Chemical Industries, Ltd.) solution for different times (0.5–4 h) under air atmosphere at room temperature. After immersing, the samples were filtered under reduced pressure by millipore filter (0.1 μm φ) and washed by distilled water. After that, they were dried at 100 °C for 24 h and we obtained delithiated samples of $Li_xNi_{0.5}Mn_{0.5}O_2$ ($0.50 \le x < 1.00$).

2.2. Characterization

Phases of samples were identified by powder XRD (CuKα: X'Pert Pro, PANalytical), and lattice parameters were calculated using layered rock-salt α-$NaFeO_2$ structure (space group: $R\bar{3}m$). The composition of metal components was analyzed by ICP-AES (ICPS-7500, Shimadzu Co.), and the metal composition was normalized so that total number of Ni + Mn was equal to 1. To measure the valence change according to delithiation, valence of Ni + Mn was measured by potentiometric titration using $KMnO_4$. Then, amount of oxygen were determined by metal composition and valence of Ni + Mn. We measured SEM (S-2600N, Hitachi) to observe the grain size and morphology of samples. Thermodynamic stability of samples were measured by twin-type multi-calorimeter (NMC-5111, Tokyo Riko Co.) [23].

2.3. Crystal structure

2.3.1. X-ray absorption spectroscopy

XAFS was measured by using synchrotron X-ray (BL9A, BL12C, KEK-PF). Ni K-edge and Mn K-edge spectra were measured with transmission mode at room temperature and analyzed by using REX2000 (Rigaku Co.). For EXAFS analysis, Fourier transform of $\chi(k)$ weighted k^3 was calculated in the range of k = 3.0–14.5 (Ni) and k = 3.0–15.0 (Mn).

2.3.2. Rietveld analysis

The crystal structure was studied by powder neutron diffraction (λ = 0.18204 nm: HERMES, JRR-3) and synchrotron XRD (λ = 0.05004 nm: BL19B2, SPring-8) at room temperature. We performed Rietveld analysis [30] by RIETAN-FP [31], and considered cation mixing to refine occupancy of 3a and 3b site [space group: $R\bar{3}m$ (3a: Li/Ni; 3b: Ni/Mn/Li; 6c: O)]. The bond length, bond angle, quadratic elongation (λ) [32], bond angle variance (σ^2) [32] and bond valence sum (B.V.S.) [33,34] were calculated by VESTA [35]. Furthermore, the nuclear densities and electron densities were analyzed by the maximum entropy method (MEM) (program PRIMA [36]) using neutron diffraction and synchrotron XRD data.

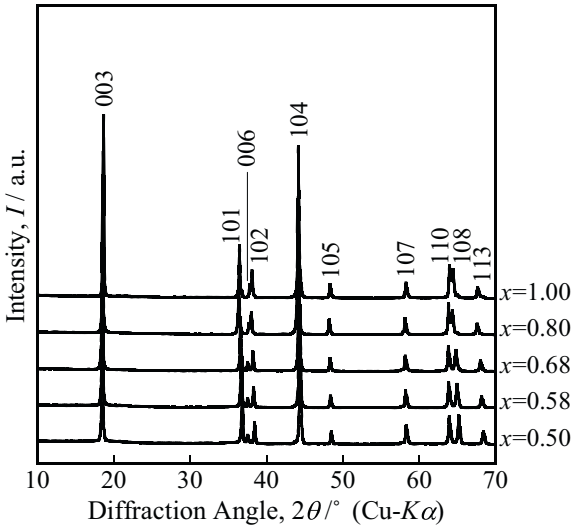

Fig. 1. Powder XRD pattern of $Li_xNi_{0.5}Mn_{0.5}O_2$ samples.

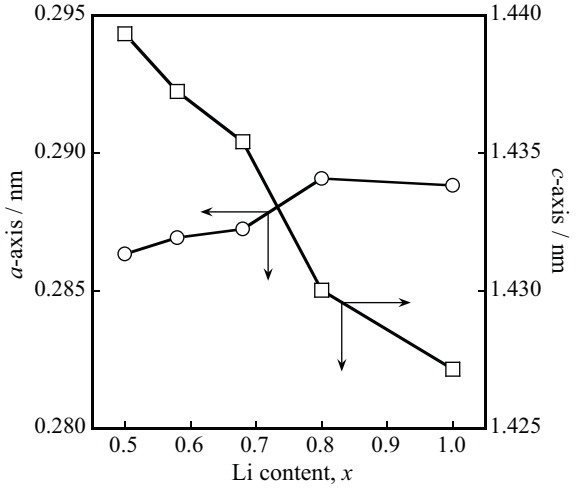

Fig. 2. Relationship between lattice parameter and Li content, x of $Li_xNi_{0.5}Mn_{0.5}O_2$. ○: a-axis; □: c-axis.

3. Results and discussion

3.1. Characterization

Fig. 1 shows powder XRD pattern of $Li_xNi_{0.5}Mn_{0.5}O_2$ samples made from $LiNi_{0.5}Mn_{0.5}O_2$. All samples were defined as α-$NaFeO_2$ structure and there was no change by chemical delithiation process. Fig. 2 shows lattice constants of the samples calculated by XRD pattern. The length of a-axis decreased and that of c-axis increased by delithiation. According to previous reports [37], decrease of a-axis has occurred from decrease of effective ionic radius [38] caused by increase of valence of transition metal, and increase of c-axis has occurred from increase of electrostatic repulsion of O–O by delithiation. Table 1 shows sample composition and average valence of Ni + Mn of each sample by ICP-AES and potentiometric titration. For

Table 1
Composition and average valence of Ni + Mn.

x	Metal composition			Oxygen content	Ni + Mn valence
	Li	Ni	Mn		
1.00	0.9920(9)	0.5116(1)	0.4884(8)	1.973	2.954(7)
0.80	0.7982(1)	0.5151(5)	0.4849(7)	1.872	2.945(1)
0.68	0.683(1)	0.509(1)	0.491(1)	1.904	3.125(3)
0.58	0.582(1)	0.5133(1)	0.4867(3)	1.883	3.183(5)
0.50	0.4963(8)	0.5094(6)	0.4906(1)	1.885	3.274(5)

metal composition, Li content was decreased, but Ni and Mn was almost constant after the chemical delithiation. From this result, it can remove Li without the elution of the transition metal by using $(NH_4)_2S_2O_8$. In addition, we calculated oxygen content from metal composition and valence of Ni + Mn. One could observe decrease of oxygen like O_2 removal at $0.80 \leq x \leq 1.00$ without increase of valence of Ni + Mn, and this phenomena is very interesting. In $0.50 \leq x \leq 0.80$, oxygen content was almost constant and valence of Ni + Mn increased by delithiation, and so it duplicates electrochemical charge. Fig. 3 shows SEM images of $Li_xNi_{0.5}Mn_{0.5}O_2$ before and after the process. Grain size of the sample did not show any change by delithiation although it seems grain surface became smooth due to washing process of chemical delithiation.

In XRD pattern, the split of 006/012 and 110/108 peaks changed clearly by chemical delithiation treatment, and this tendency observed in this work was the same with NO_2BF_6 treatment by Venkatraman et al. [27]. In other words, the changes of lattice parameters were the same in these studies; *a* axis decreased and *c*-axis increased. On the other hand, the behavior of oxygen was different. In this study, oxygen was removed at $0.8 \leq x \leq 1.0$, but Venkatraman et al. [27] reported that oxygen was removed at $0 \leq x \leq 0.5$. Such a difference may be a result of using a different oxidizing agent for $LiNi_{0.5}Mn_{0.5}O_2$.

3.2. Thermodynamic stability

The thermodynamic stability of the oxide is usually evaluated by the Gibbs free energy, ΔG. The value of $T\Delta S$ in $\Delta G = \Delta H - T\Delta S$ is negligible because of the reaction is solid phase at room temperature in this study. So thermodynamic stability can evaluated by ΔH [23,39–41]. When comparing enthalpies between oxides with different number of atoms in the chemical formula unit, difference of the number of atoms may affect standard enthalpy of formation, $\Delta_f H_0$ and enthalpy changes of reaction. So in this study, the thermodynamic stability was evaluated by utilizing the enthalpy change per mole of atoms for the formation reaction, ΔH_R [21]. ΔH_R can be calculated by Eq. (1).

$$\Delta H_R = \frac{\Delta_f H^\circ(Li_xNi_{0.5}Mn_{0.5}O_2)}{\nu} - \frac{\sum \Delta_f H^\circ(Li_2O,NiO,MnO_2)}{\nu} \quad (1)$$

$\Sigma\Delta_f H^\circ$ term is the sum of the standard enthalpies of formation of each simple oxide and ν is the number of moles of atoms in one mole of material [23,42,43]. Fig. 4 shows the relationship between ΔH_R and the Li content, x of $Li_xNi_{0.5}Mn_{0.5}O_2$. ΔH_R was increased linearly with delithiation. This result means that there is no phase transition by chemical delithiation, and it corresponds to XRD results.

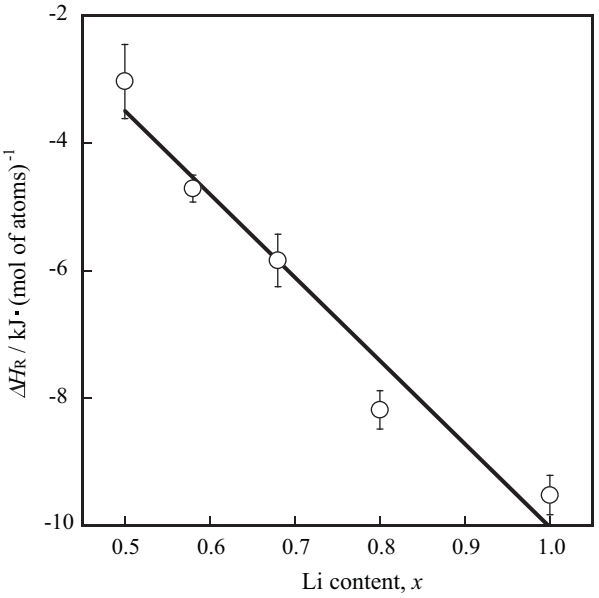

Fig. 4. Relationship between the enthalpy change per mole of atoms for formation reaction, ΔH, and Li content, x of $Li_xNi_{0.5}Mn_{0.5}O_2$.

3.3. Structure analysis

3.3.1. XAS

Fig. 5 shows Ni and Mn K-edge XANES spectra by synchrotron X-ray. The spectra profiles changed by delithiation. Ni K-edge peak shifted to higher energy, so valence of Ni increased by delithiation.

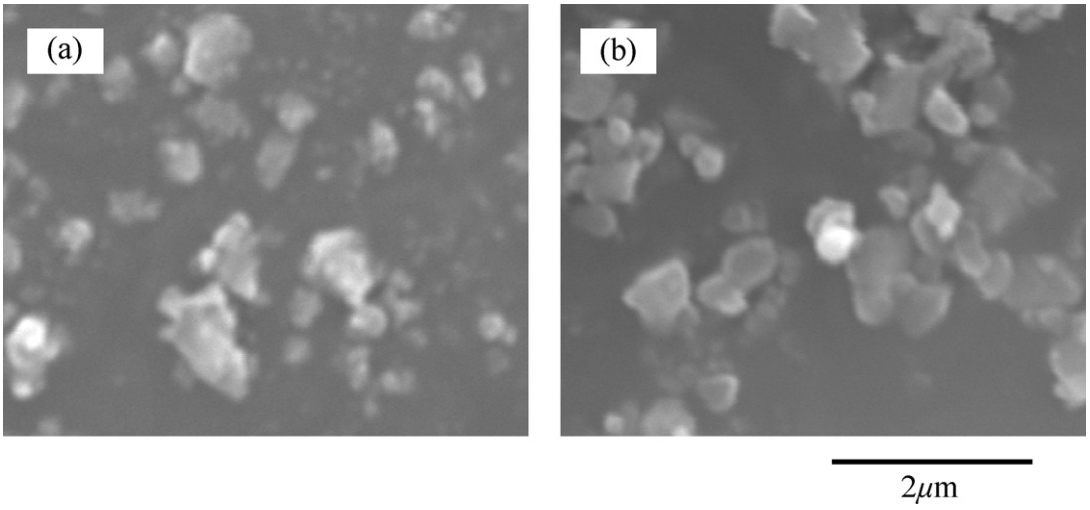

Fig. 3. SEM image of $Li_xNi_{0.5}Mn_{0.5}O_2$ particles of $Li_xNi_{0.5}Mn_{0.5}O_2$. (a) Before delithiation (x = 1.00), (b) after delithiation (x = 0.50).

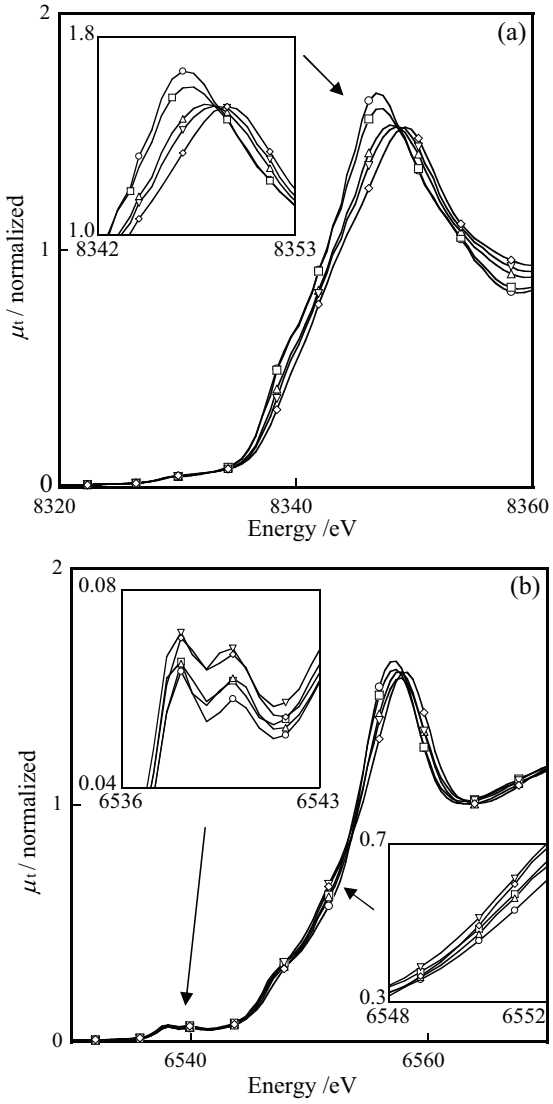

Fig. 5. (a) Ni K-edge and (b) Mn K-edge XANES spectra of $Li_xNi_{0.5}Mn_{0.5}O_2$. ○: $x = 1.00$; □: $x = 0.80$; △: $x = 0.68$; ▽: $x = 0.58$; ◇: $x = 0.50$.

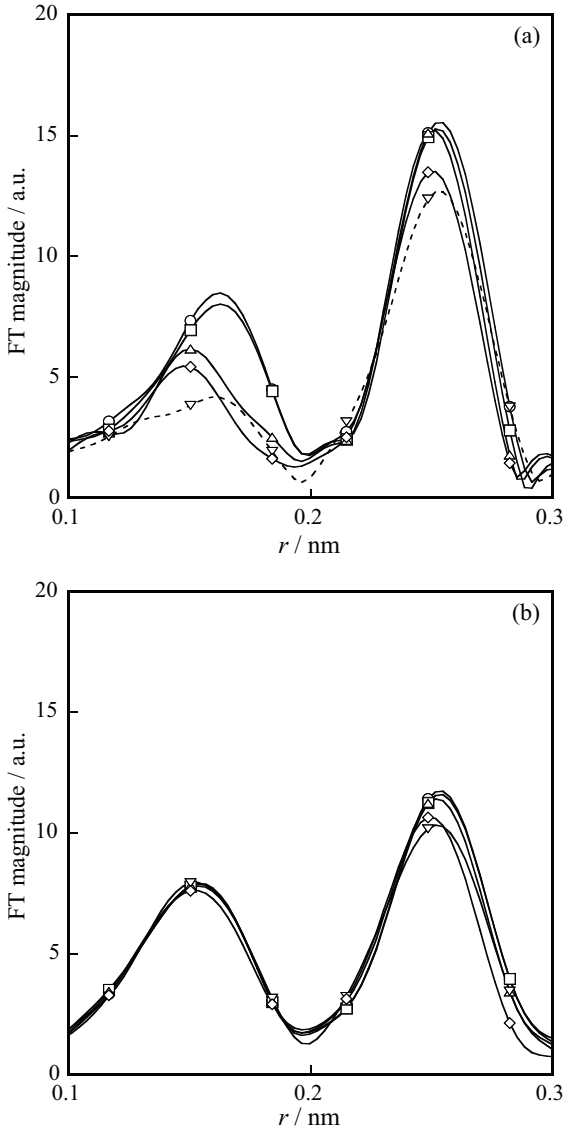

Fig. 6. (a) Ni K-edge and (b) Mn K-edge EXAFS spectra of $Li_xNi_{0.5}Mn_{0.5}O_2$. ○: $x = 1.00$; □: $x = 0.80$; △: $x = 0.68$; ▽: $x = 0.58$; ◇: $x = 0.50$.

On the other hand, Mn K-edge peak did not shift although the peak profile changed. This result was caused by changes of coordination state, not valence of Mn. These changes of XANES spectra correspond to the result of in situ measurement of electrochemically charged samples [16–18].

Fig. 6 shows EXAFS spectra of Ni and Mn K-edge. In 1st coordination of Ni (Ni–O), Ni–O bond length decreased and distortion of Ni–O_6 octahedra increased by delithiation. Contrarily there was no change by delithiation in 1st coordination of Mn (Mn–O). In the case of electrochemical charge [17], Ni 1st coordination showed different changes which occurred from production of Ni^{4+} at lower Li content than 0.6–0.7. Such a difference may be originated from the O_2 removal reaction in the initial chemical delithiation process ($0.80 \leq x \leq 1.00$) shown in Table 1. That is, due to the O_2 removal, Ni valence was still below trivalent even after the chemical delithiation proceeded until $x = 0.5$. M–M distances were slightly decreased by delithiation at Ni and Mn 2nd coordination (Ni–M, Mn–M). It seems that decrease of ionic radius according to increase of Ni valence affects distance of Mn–Ni, and thus each 2nd coordination shows this behavior. The same behavior of peak shift of 2nd coordination was also reported in electrochemical charge [17] although the change of peak height showed slight difference. In the chemical delithiation treatment, peak height was almost constant at $0.68 \leq x \leq 1.00$, and decreased at $0.50 \leq x \leq 0.68$. On the other hand, each Ni and Mn peak height decreased at $0.6–0.7 \leq x \leq 1.0$, and then increased when the Li content was below them in the case of electrochemical charge [17].

As shown in Table 1, there is O_2 removal process, which corresponds to 0.2 Li (from 1.00 to 0.80) in chemical delithiation. Because of this process, the structure changes versus amount of delithiation were slightly different between the chemical delithiation and the electrochemical delithiation at $0.80 \leq x \leq 1.00$. On the other hand, the tendency of changes of electronic structure (XANES) and local structures (EXAFS) corresponded to the previous results by electrochemical charge [16,17] at $0.50 \leq x \leq 0.80$. In order to investigate structure change during charge–discharge cycle in more detail, we performed neutron diffraction measurements of the chemically delithiated samples in the following section.

3.3.2. Crystal structure analysis

We refined the crystal structure of $Li_xNi_{0.5}Mn_{0.5}O_2$ to investigate change of structure by Rietveld analysis using powder neutron diffraction and powder synchrotron XRD. Space group $R\bar{3}m$ was

Table 2
Occupancy of Ni(3a), Li(3b) and *R*-factor of Rietveld refinement.

x	(a) Neutron			(b) Synchrotron		
	Ni(3a)	Li(3b)	R_{wp}	Ni(3a)	Li(3b)	R_{wp}
1.00	0.097(2)	0.097(2)	6.328	0.098(1)	0.098(1)	7.18
0.80	0.070(3)	0.071(3)	4.897	0.085(1)	0.085(1)	8.33
0.68	0.079(2)	0.079(2)	5.380	0.075(1)	0.075(1)	5.39
0.58	0.099(2)	0.099(2)	4.906	0.081(1)	0.081(1)	7.55
0.50	0.118(2)	0.118(2)	4.705	0.095(1)	0.095(1)	7.76

Table 3
Bond length, bond angle and *z* of O (neutron diffraction).

x	Bond length (nm)		Bond angle (°)	*z*(6c)	Oxygen content
	3a–6c	3b–6c	3a–6c–3b		
1.00	0.2111(1)	0.19841(9)	175.0(1)	0.2423(1)	1.953(9)
0.80	0.2121(1)	0.1991(1)	174.9(1)	0.2422(2)	1.87(1)
0.68	0.21348(9)	0.19709(8)	173.6(1)	0.2403(1)	1.900(8)
0.58	0.21375(8)	0.19633(7)	173.2(1)	0.23965(9)	1.889(8)
0.50	0.21399(8)	0.19516(7)	172.7(1)	0.23884(9)	1.883(8)

Table 4
B.V.S. and valence of 3a, 3b site calculated by analytical valence and occupancy.

x	B.V.S.		Valence	
	3a	3b	3a	3b
1.00	1.11	2.71	1.09	2.86
0.80	1.07	2.65	1.09	2.87
0.68	1.04	2.90	1.12	3.05
0.58	1.07	2.98	1.17	3.09
0.50	1.10	3.11	1.24	3.16

used for refinement because XRD patterns of all samples could be defined by α-$NaFeO_2$ structure (Fig. 1) and thermodynamic results (ΔH_R) showed linear data (Fig. 4). Table 2 shows occupancy of Ni at 3a site and Li at 3b site which means amount of cation mixing, and shows goodness of fitting of refinement, R_{wp}. R_{wp} shows low value in each result by using space group $R\bar{3}m$, and it suggests that there was no phase transition. Furthermore, the occupancy of Li at 3b site was essentially constant, so it can be considered that Li deintercalates from only 3a site by chemical delithiation. Table 3 shows 3a–6c, 3b–6c bond length, 3a–6c–3b bond angle and oxygen content calculated from analyzed structure parameter. 3a–6c bond length increased and 3b–6c bond length decreased with delithiation. It suggests that increase of electrostatic repulsion of O(6c)–O(6c) due to delithiation has an effect on 3a–6c bond length which relates to inter transition-metal's slab space (I_{LiO_2} [44]). On the other hand, decrease of effective ionic radius due to increase of valence of Ni affects 3b–6c bond length which relates to the slab thickness (S_{MO_2} [44]). 3a–6c–3b bond angle decreased by delithiation, and this reflects that O ($z \approx 0.24$) shifts to 3b site side ($z = 1/6$) from 3a site side ($z = 1/3$) by increase of I_{LiO_2} and decrease of S_{MO_2}. Oxygen content was calculated by refinement occupancy of oxygen. Compared with the analytical oxygen content (Table 1), each result showed approximately same in each sample. Therefore, Rietveld refinement of neutron diffraction data suggests the O_2 removal in $0.80 \leq x \leq 1.00$, too.

And then, we investigated to 3a–O_6, 3b–O_6 octahedra. Fig. 7 shows the distortion of octahedra and Table 4 shows B.V.S. This table also listed average valence of 3a site and 3b sites calculated from the site occupancies and the transition-metal valences estimated by the titration (Table 1). In the calculation, we also assumed that Li is monovalent and Ni at 3a site is divalent. Distortion of bond lengths, λ and distortion of bond angles, σ^2 increased with delithiation in each octahedra. Especially, increase of the distortion was remarkable at 3a–O_6 octahedra. Increase of I_{LiO_2} with delithiation is one of the reasons, but vacancy of Li generated by deintercalation from 3a site also influences the distortions greatly. From the EXAFS results (Fig. 6), the distortion of 3b–O_6 octahedra could be attributed to Ni–O change, whereas Mn–O_6 octahedra may be a structural pillar. Next, B.V.S., which shows effective valence of cation, showed almost constant at 3a site and increased at 3b site. Taking into account this result in addition to the fact that Mn valence was almost constant from results of XANES (Fig. 5), valence of Ni increased only at 3b site without any changes at 3a site. Furthermore, B.V.S. corresponded to valence calculated from analytical valence of Ni + Mn and occupancy of each sites (3a: Li + Ni; 3b: Ni + Mn + Li). This result ensures a validity of the crystal structure refinement.

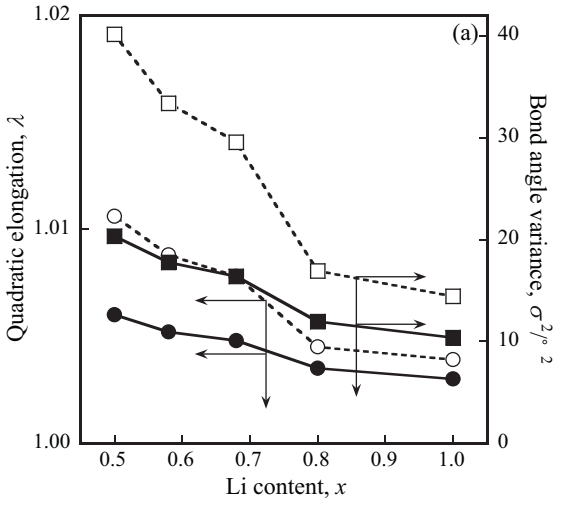

Fig. 7. Distortion of 3a–O_6 (○, □), 3b–O_6 (●, ■) octahedra of $Li_xNi_{0.5}Mn_{0.5}O_2$. ○, ●: quadratic elongation; □, ■: bond angle variance.

Table 5
Nuclear density of each site by MEM.

x	3a	3b	6c
1.00	−2.804	78.35	106.24
0.80	−1.500	109.64	205.36
0.68	−0.702	82.70	173.97
0.58	−0.065	66.29	177.70
0.50	5.297	52.43	166.95

However, the changes of crystal structure by chemical delithiation showed some differences with electrochemical delithiation (charge). Arachi et al. reported the phase transition to space group C2/m by electron diffraction and synchrotron XRD [13]. But, there was no phase transition at $0.50 \leq x \leq 1.00$ range by chemical delithiation treatment in this study. The O_2 removal was confirmed at $0.80 \leq x \leq 1.00$ (Table 1), and it may affect the difference from electrochemical charge. Bréger et al. could not detect such a phase transition in charged samples, and concluded that it related to the resolution of experiments or slight difference of the samples [20]. Moreover, according to the report, decrease of Li at 3b site was reported by structure analysis using neutron TOF diffraction. Considering these, a further investigation with in situ neutron diffraction measurements is necessary.

3.3.3. Nuclear and electron density by MEM

We investigated the nuclear density distribution by MEM using refinement structure data for powder neutron diffraction measurements. Table 5 shows nuclear density at 3a, 3b and 6c sites. Nuclear density at 3a site increased with delithiation. Each coherent scattering length of Li and Ni are −1.90 and 10.3, so this result supports

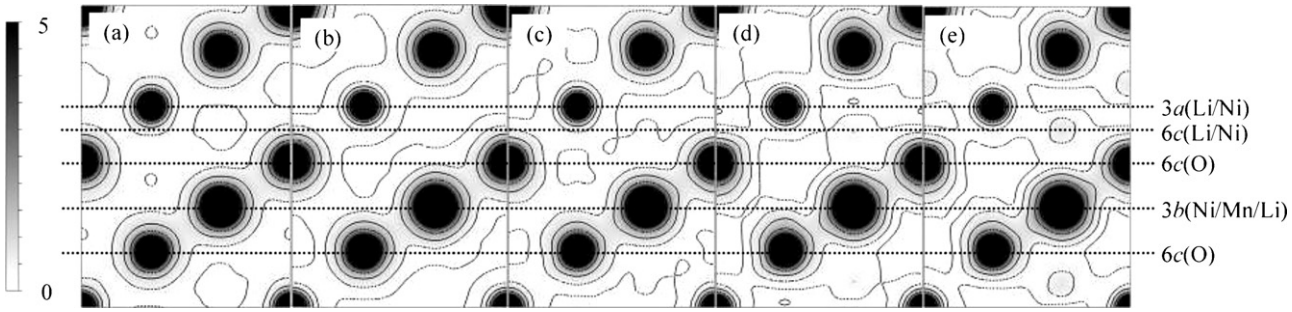

Fig. 8. Electron density distribution of $Li_xNi_{0.5}Mn_{0.5}O_2$. Contour line $F(N)$; $1 \times 10^{N/step}$, $N = -1$ to 1, step = 3. (a) $x = 1.00$; (b) $x = 0.80$; (c) $x = 0.68$; (d) $x = 0.58$; (e) $x = 0.50$

the delithiation from 3a site and existence of Ni at 3a site. Moreover, nuclear densities at 3b and 6c site were almost constant even after delithiation. This indicates that the host structure was stable and amount of cation mixing did not change by delithiation.

Additionally, we investigated the electron density distribution by using synchrotron XRD measurements. Fig. 8 shows electron density distribution of (1 1 0) plane. Electron density between 3b and 6c was increased by delithiation. This result means 3b–6c covalent bond got stronger by delithiation. Such a covalent character may relax structure instability by delithiation. It was also found that there were electron density at another position than 3a, 3b and 6c site. This position was tetrahedral site (6c; 0, 0, $z \approx 0.38$) [not equal to O site (6c; 0, 0, $z \approx 0.24$)]. Kobayashi et al. [15] and Breger et al. [20] reported the existence of 10–20% Li and 1–5% Ni on this tetrahedral site by using synchrotron XRD and neutron diffraction. Based on these previous reports, this electron density may be attributable to Li and/or Ni, and it suggests the migration of these metals by chemical delithiation treatment.

4. Conclusion

Chemical delithiation using ammonium peroxodisulfate could reproduce electrochemical delithiation (charge process) in terms of bond length, displacement of O (Rietveld analysis), local structure (EXAFS) and electronic structure (XANES, MEM). Thermodynamic data changed linearly with delithiation, so there was no phase transition by delithiation ($0.50 \leq x \leq 1.00$). From structure analyses, Li deintercalated from only 3a site and the redox was happen Ni at 3b site. The cation mixing of Li(3b) and Ni(3a) did not take part in deintercalation and redox. The distortion of M(3b)–O_6 octahedra increased by delithiation, which was caused by Ni–O bond change. However chemical delithiation treatment accompanied O_2 removal at $0.80 \leq x \leq 1.00$, in contrast to electrochemical delithiation. And the determination of the O_2 removal mechanism is an examination issue for the future.

Acknowledgement

The authors thank Prof. Y. Uchimoto of Kyoto Univ. for his technical assistance in the XAS measurements.

References

[1] K. Mizushima, P.C. Jone, P.J. Wiseman, J.B. Goodenough, Mater. Res. Bull. 15 (1980) 783.
[2] M.M. Thackeray, R.J. Johnson, L.A. de Picciotto, P.G. Bruce, J.B. Goodenough, Mater. Res. Bull. 19 (1984) 179.
[3] A.K. Padhi, K.S. Nanjundaswamy, J.B. Goodenough, J. Electrochem. Soc. 144 (1997) 1188.
[4] T. Ohzuku, Y. Makimura, Chem. Lett. 7 (2001) 642.
[5] T. Ohzuku, Y. Makimura, Chem. Lett. 30 (2001) 744.
[6] Y. Makimura, T. Ohzuku, J. Power Sources 119 (2003) 156.
[7] A. Van der Ven, G. Ceder, Electrochem. Commun. 6 (2004) 1045.
[8] J. Bréger, N. Dupré, P.J. Chupas, P.L. Lee, T. Proffen, J.B. Parise, G. Ceder, C.P. Grey, J. Am. Chem. Soc. 127 (2005) 7529.
[9] H.H. Li, N. Yabuuchi, Y.S. Meng, S. Kumar, J. Breger, C.P. Grey, Y. Shao-Horn, Chem. Mater. 19 (2007) 2551.
[10] N. Yabuuchi, S. Kumar, H.H. Li, Y.-T. Kim, Y. Shao-Horn, J. Electrochem. Soc. 154 (2007) A566.
[11] Y.S. Meng, G. Ceder, C.P. Grey, W.-S. Yoon, Y. Shao-Horn, Electrochem. Solid-State Lett. 7 (2004) A155.
[12] J. Bréger, K. Kang, J. Cabana, G. Ceder, C.P. Grey, J. Mater. Chem. 17 (2007) 3167.
[13] Y. Arachi, H. Kobayashi, S. Emura, Y. Nakata, M. Tanaka, T. Asai, H. Sakaebe, K. Tatsumi, H. Kageyama, Solid State Ionics 176 (2005) 895.
[14] K. Sakamoto, M. Hirayama, H. Konishi, N. Sonoyama, N. Dupré, D. Guyomard, K. Tamura, J. Mizuki, R. Kanno, Phys. Chem. Chem. Phys. 12 (2010) 3815.
[15] H. Kobayashi, Y. Arachi, H. Kageyama, K. Tatsumi, J. Mater. Chem. 14 (2004) 40.
[16] H. Nakano, T. Nonaka, C. Okuda, Y. Ukyo, J. Ceram. Soc. Jpn. 111 (2003) 33.
[17] W.-S. Yoon, C.P. Grey, M. Balasubramanian, X.-Q. Yang, J. McBreen, Chem. Mater. 15 (2003) 3161.
[18] A. Deb, U. Bergmann, S.P. Cramer, E.J. Cairns, J. Appl. Phys. 99 (2006) 63701.
[19] N.K. Karan, J.J. Saavedra-Arias, D.K. Pradhan, R. Melgarejo, A. Kumar, R. Thomas, R.S. Katiyar, Electrochem. Solid-State Lett. 11 (2008) A135.
[20] J. Bréger, Y.S. Meng, Y. Hinuma, S. Kumar, K. Kang, Y. Shao-Horn, G. Ceder, C.P. Grey, Chem. Mater. 18 (2006) 4768.
[21] O. Sekizawa, N. Kitamura, Y. Idemoto, Electrochemistry 78 (2010) 367.
[22] M.S. Islam, R.A. Davies, J.D. Gale, Chem. Mater. 15 (2003) 4280.
[23] Y. Idemoto, T. Matsui, Solid State Ionics 179 (2008) 625.
[24] W. Tang, H. Kanoh, K. Ooi, J. Solid State Chem. 142 (1999) 19.
[25] R.V. Chebiam, A.M. Kannan, F. Prado, A. Manthiram, Electrochem. Commun. 3 (2001) 624.
[26] J. Bang, H. Joachin, H. Yang, K. Amine, J. Prakash, J. Electrochem. Soc. 153 (2006) A731.
[27] S. Venkatraman, A. Manthiram, Chem. Mater. 15 (2003) 5003.
[28] C.-H. Chen, B.-J. Hwang, C.-Y. Chen, S.-K. Hu, J.-M. Chen, H.-S. Sheu, J.-F. Lee, J. Power Sources 174 (2007) 938.
[29] Y. Idemoto, K. Horiko, Y. Ito, N. Koura, K. Ui, Electrochemistry 72 (2004) 755.
[30] H.M.J. Rietveld, Appl. Crystallogr. 2 (1969) 65.
[31] F. Izumi, T. Ikeda, Mater. Sci. Forum 198 (2000) 321.
[32] K. Robinson, G.V. Gibbs, P.H. Ribbe, Science 172 (1971) 567.
[33] I.D. Brown, D. Altermatt, Acta Crystallogr. Sect. B 41 (1985) 244.
[34] N.E. Brese, M. O'Keeffe, Acta Crystallogr. Sect. B 47 (1991) 192.
[35] K. Momma, F. Izumi, J. Appl. Crystallogr. 41 (2008) 653.
[36] F. Izumi, J. Crystal. Soc. Jpn. 44 (2002) 380.
[37] J. Choi, A. Mnathiram, J. Electrochem. Soc. 152 (2005) A1714.
[38] R.D. Shannon, Acta Crystallogr. A32 (1976) 751.
[39] Y. Idemoto, Y. Yasuda, K. Fueki, Physica C 243 (1995) 35.
[40] Y. Idemoto, H. Tokue, K. Fueki, Physica C 243 (1995) 43.
[41] Y. Idemoto, I. Oyagi, K. Fueki, Physica C 199 (1992) 207.
[42] Y. Idemoto, K. Konnno, K. Ui, N. Koura, Electrochemistry 73 (2005) 823.
[43] Y. Idemoto, K. Horiko, K. Ui, N. Koura, Electrochemistry 72 (2004) 680.
[44] M. Guilmard, L. Croguennec, C. Delams, J. Electrochem. Soc. 150 (2003) A1287.